J|A|C|S

Flipping in the Pore: Discovery of Dual Inhibitors That Bind in Different Orientations to the Wild-Type versus the Amantadine-Resistant S31N Mutant of the Influenza A Virus M2 Proton Channel

Yibing Wu,[†,○] Belgin Canturk,[‡,○] Hyunil Jo,[†,○] Chunlong Ma,[∇] Eleonora Gianti,[#] Michael L. Klein,[#] Lawrence H. Pinto,[§] Robert A. Lamb,[‖,⊥] Giacomo Fiorin,*[#] Jun Wang,*[∇] and William F. DeGrado*[†]

[†]Department of Pharmaceutical Chemistry, University of California, Mission Bay Box 3122, San Francisco, California 94158, United States

[‡]Department of Chemistry, University of Pennsylvania, 231 South 34th Street, Philadelphia, Pennsylvania 19104, United States

[§]Department of Neurobiology, Northwestern University, 2205 Tech Drive, Evanston, Illinois 60208, United States

[‖]Department of Molecular Biosciences, Northwestern University, 2205 Tech Drive, Evanston, Illinois 60208, United States

[⊥]Howard Hughes Medical Institute, Northwestern University, Evanston, Illinois 60208, United States

[#]Institute for Computational and Molecular Science, Science Education and Research Center (035-07), Temple University, 1925 North 12th Street, Philadelphia, Pennsylvania 19122, United States

[∇]Department of Pharmacology and Toxicology and the BIO5 Institute, The University of Arizona, 1501 N. Campbell Avenue, Tucson, Arizona 85721, United States

S *Supporting Information*

ABSTRACT: Influenza virus infections lead to numerous deaths and millions of hospitalizations each year. One challenge facing anti-influenza drug development is the heterogeneity of the circulating influenza viruses, which comprise several strains with variable susceptibility to antiviral drugs. For example, the wild-type (WT) influenza A viruses, such as the seasonal H1N1, tend to be sensitive to antiviral drugs, amantadine and rimantadine, while the S31N mutant viruses, such as the pandemic 2009 H1N1 (H1N1pdm09) and seasonal H3N2, are resistant to this class of drugs. Thus, drugs targeting both WT and the S31N mutant are highly desired. We report our design of a novel class of dual inhibitors along with their ion channel blockage and antiviral activities. The potency of the most active compound **11** in inhibiting WT and the S31N mutant influenza viruses is comparable with that of amantadine in inhibiting

WT influenza virus. Solution NMR studies and molecular dynamics (MD) simulations of drug-M2 interactions supported our design hypothesis: namely, the dual inhibitor binds in the WT M2 channel with an aromatic group facing down toward the C-terminus, while the same drug binds in the S31N M2 channel with its aromatic group facing up toward the N-terminus. The flip-flop mode of drug binding correlates with the structure—activity relationship (SAR) and has paved the way for the next round of rational design of broad-spectrum antiviral drugs.
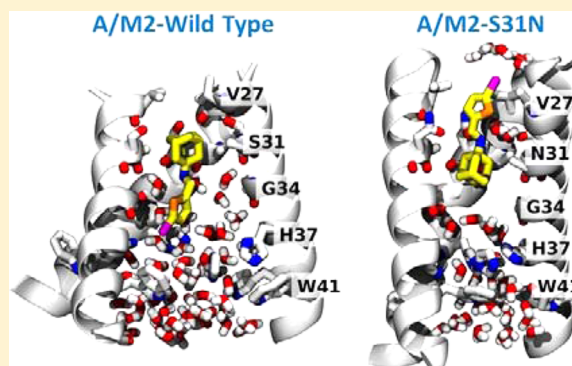
■ INTRODUCTION

Influenza virus infection poses a global health and economic challenge that has yet to be addressed.[1] During an annual influenza season, an estimate of 35 000 people die due to influenza-related illnesses, which places influenza among top 10 leading causes of death in the U.S.[2,3] What is more alarming is the emergence of highly pathogenic avian influenza (HPAI) strains, such as H5N1,[4] and more recently the H7N9,[5] which have much higher mortality rate than seasonal influenza strains. It has been shown that these HPAI strains need to acquire only one or a few mutations to become transmissible among humans, which raises the likelihood of the next influenza pandemic.[6] There are currently two classes of approved anti-

influenza drugs: M2 channel blockers (amantadine and rimantadine) and neuraminidase inhibitors (oseltamivir and zanamivir).[7] Resistance to both classes of drugs raises great concern: resistance to M2 inhibitors is so prevalent that the Centers for Disease Control and Prevention (CDC) recommended discontinued use of this class of drugs, and resistance to the only orally bioavailable drug oseltamivir was dominant in the 2007—2008 influenza season.[8,9] This leaves zanamivir as the last resort of treatment; however, the low bioavailability and its nasal route of administration limit its use in severely ill

patients.[10] Thus, there is a great need for the next generation of orally bioavailable antiviral drugs.[11] One challenge facing anti-influenza drug development is the heterogeneous makeup of the circulating influenza viruses, which comprise several influenza strains with different susceptibilities to antiviral drugs. For example, among the influenza viruses in recent influenza seasons, the H1N1pdm09 and seasonal H3N2 strains are oseltamivir-susceptible and amantadine-resistant, while the seasonal H1N1 strains are mostly oseltamivir-resistant and amantadine-susceptible.[12,13] Moreover, influenza viruses continue to evolve, and it is almost impossible to predict the drug susceptibility of a novel influenza strain.[14,15] As an illustration, the H5N1 strains isolated from Vietnam, Thailand, and Cambodia have the characteristic S31N mutation, which confers amantadine resistance.[16] However, strains isolated from other countries, such as China, Indonesia, Japan, and Korea, mostly carry the WT M2 and remain susceptible to amantadine. From the drug discovery standpoint, it would be ideal to develop broad-spectrum antiviral drugs that are active against multiple influenza virus strains, thus circumventing the need of combination therapy which often has drug–drug interaction-related issues.[17] Herein, we focus on M2 as a drug target and report the design of a novel class of M2 channel blockers that are active against both the WT and the S31N mutant.

The influenza A virus M2 protein (A/M2) is a virus-encoded proton channel that plays multiple roles during the viral replication cycle: in the early stage of virus uncoating, M2 facilitates unpacking of viral RNAs by acidifying the viral interior; in the late stage of viral replication, M2 equilibrates the pH across the Golgi apparatus in order to prevent premature conformational changes of another viral surface protein-hemagglutinin.[18] M2 is a validated drug target of antiviral drugs, amantadine and rimantadine. However, mutations surrounding the drug binding site, such as S31N, V27A, A30T, and L26F, lead to escape of drug inhibition.[19] In cell cultures, a large number of drug-resistant M2 mutants readily emerged under amantadine drug selection pressure.[20–22] A subset of these mutations was also observed in influenza-infected patients following treatment with amantadine.[23] Reverse-engineered viruses harboring various pore-lining mutations were competent to replicate in mice,[24] raising concerns that M2 might not be an ideal antiviral target. However, electrophysiological investigations showed that the majority of the resulting amantadine-resistant M2 channels had shifts in their conductance characteristics that might render the viruses less fit.[25,26] This is probably because even minor changes of one amino acid side chain lead to four changes in M2's 4-fold symmetric homotetrameric pore. Indeed, many of these M2 mutations gave somewhat attenuated viruses that have a tendency to revert to the WT M2 in the absence of drug pressure and do not appear to be highly transmissible.[22,27] Corroborating observations in cell cultures, large-scale sequencing of transmissible viruses from 1918 to 2008 have identified only three major amantadine-resistant M2 mutants, S31N, V27A, and L26F.[28,29] Among these three drug resistant mutants, S31N is the predominant mutant and persists in more than 95% of currently circulating influenza viruses. Drug discovery efforts targeting these M2 mutants have long been hampered because of the lack of high-resolution structures, the constricted drug binding site, and the dynamic nature of this protein.[30] Nevertheless, progress has been made in designing inhibitors targeting the drug-resistant mutants of M2 guided by

MD simulations[31–36] and NMR structures M2.[37–40] The designed small molecule channel blockers inhibit V27A, L26F, and S31N M2 with potencies greater than that of amantadine in both electrophysiological assays and antiviral plaque reduction assays. These inhibitors not only represent excellent leads for further development, but also help stabilize the otherwise dynamic M2 protein, leading to the determination of the first high resolution solution NMR structure of the A/M2-S31N mutant.[36] Herein, we describe the extension of these studies to design dual inhibitors targeting both WT and the S31N mutant. Such broadly specific antiviral drugs are superior to mutant-selective inhibitors: ideally, a single drug will be sufficient to combat multiple circulating influenza virus strains, thereby alleviating the need for combination therapy as required when treating human immunodeficiency virus (HIV) infections.[41]

◼ MATERIALS AND METHODS

Materials. All starting materials for compound and peptide synthesis were purchased from commercial vendors and used without purification, unless otherwise stated. Reactions were carried out using HPLC grade solvents under N_2 atmosphere. Compounds were purified by silica gel flash column chromatography and characterized by ESI-MS, ^1H NMR, and ^{13}C NMR.

Inhibitor Synthesis. Details about inhibitor synthesis procedures and characterization can be found in the Supporting Information.

Two-Electrode Voltage Clamp (TEVC) Assay. All compounds were initially tested in TEVC assay using *Xenopus laevis* frog oocytes microinjected with RNA expressing either the WT or the S31N mutant of M2 as described in a previous report.[32] The potency of the inhibitors was expressed as the percentage inhibition of A/M2 current observed after 2 min of incubation with 100 μM compounds, and potent inhibitors were further tested at series dilutions to quantify their IC_{50} values.

Plaque Reduction Assay. The plaque reduction assays were performed according to a previous report.[35] WT M2-expressing A/Udorn/72 and M2-S31N-expressing A/WSN/33 were used to infect MDCK cells in the presence or absence of compounds to evaluate their antiviral activity. The EC_{50}s were subsequently determined for potent dual inhibitors.

Molecular Dynamics (MD) Simulations. We used the 22–46 transmembrane segment of the tetrameric M2 protein (Udorn sequence) (M2-TM), modeled after the intermediate-pH structure of the 25–46 segments,[42] with two histidines doubly protonated and the other two in the neutral state. We embedded each complex with compound **11** in an 8 × 8 nm^2 1-palmitoyl-2-oleoylphosphatidylcholine (POPC) bilayer, hydrated by a 150 mM KCl water solution. We used the CHARMM36,[43,44] CGenFF,[45] and TIP3P[46] force fields for the treatment of M2-TM and lipids, **11**, and water molecules, respectively. We optimized the partial charge of the bromine atom of **11** by MP2 calculations, as detailed in the Supporting Information. **11** was placed in the channel with the bromo-thiophene moiety facing H37 and V27 in the WT M2-TM and S31N mutant, respectively. We performed minimization and initial equilibration of water molecules, as well as relaxation of residues 22–24, with harmonic restraints on the protein backbone and on the bound **11**. We gradually released these restraints over 50 ns of simulation followed by a 150 ns unrestrained run.

NMR Sample Preparation. HPLC purified peptides were mixed with deuterated *n*-dodecylphosphocholine (DPC) (Cambridge Isotope Laboratories) at 1:50 molar ratio in ethanol. Drug was added from the ethanol stock solution to the desired molar ratio. The resulting ethanol solution was mixed by vortexing, and the ethanol was removed by nitrogen purging. The sample was lyophilized overnight to remove residual ethanol. Next, aqueous buffer [10% D_2O in H_2O, 50 mM sodium phosphate (pH 6.8)] was added to the dried mixture and vortexed for 2 min, and the pH of the final sample was adjusted to the desired value with either NaOH or H_3PO_4. The final NMR sample

conditions are the following: for S31N, 2 mM A/M2-S31N (19−49) (monomer), 20 mM **11**, 100 mM deuterated DPC, and 50 mM sodium phosphate buffer in 10% D_2O, 90% H_2O, pH 6.8; for WT, 2 mM A/M2-WT (19−49) (monomer), 2.5 mM **11**, 100 mM deuterated DPC (Cambridge Isotope Laboratories), and 50 mM sodium phosphate buffer in 10% D_2O, 90% H_2O, pH 7.5.

Peptide Synthesis and Purification. Isotopically labeled peptides used in this study, A/M2-WT (19−49) VASIGH and A/M2-S31N (19−49) VANIG, were synthesized using the optimized solid phase synthesis protocol as described previously.[47] Peptides were purified by high performance liquid chromatography (HPLC) with a C4-Vydac reverse phase column. The purity and identity of the peptides were confirmed by analytical HPLC (>98% purity) and ESI-MS. For A/M2-WT (19−49) VASIGH, calcd MS: 1539.3 (+2), 1026.5 (+3). Obsd MS: 1539.3 (+2), 1026.5 (+3). For A/M2-S31N (19−49) VANIG, calcd MS: 1549.3 (+2H), 1033.2 (+3H). Obsd MS: 1549.3 (+2H), 1033.2 (+3H).

Solution NMR Experiments. All spectra were recorded with standard pulse sequences[48,49] at 313 K on a Bruker 800 or 900 MHz spectrometers equipped with cryogenic probes. To obtain assignments, 2D ^{15}N and ^{13}C HSQC for both WT (19−49) VASIGH and S31N (19−49) VANIG M2 in the absence/presence of **11**, and 2D $^{13}C-(^{13}C)-^{1}H$ TOCSY experiments for both M2 samples in the presence of **11** were carried out. The 2D $^{13}C-(^{13}C)-^{1}H$ TOCSY (70 ms) experiments were recorded with $t_{1,max}$ = 7 ms for the ^{13}C dimension and $t_{2,max}$ = 81 ms for the ^{1}H dimension with 32 scans. 2D $^{13}C-(^{1}H)-^{1}H$ NOESY experiments with mixing time of 150 ms were carried out with $t_{1,max}$ = 7 ms for the ^{13}C dimension and $t_{2,max}$ = 71 ms for the ^{1}H dimension, 128 scans. The ^{1}H carrier frequency was set to the water signal. Chemical shifts were referenced with respect to the residual water peak at 4.63 ppm, and ^{13}C and ^{15}N chemical shifts were referenced indirectly via gyromagnetic ratios. All spectra were processed and analyzed using the nmrPipe program.[50] The time domain data of indirect ^{13}C or ^{15}N dimensions were extended once by linear prediction. The time domain data were multiplied by sine square bell window functions shifted by 90° and zero-filled once before Fourier transformation.

NOE Assignment and Model Calculation. The 2D ^{13}C-edited NOESY allows observation of NOEs from the protons that are directly attached to the ^{13}C atoms to any protons that are within approximately 5 Å, so both peptide−drug and peptide−peptide NOEs are present in a given experiment. Also, although the drug is not ^{13}C labeled, intramolecular NOEs originated from its protons attached to ^{13}C at natural abundance (1.1%) can be observed due to the fact that the drug is in large molar excess and the free drug has favorable relaxation properties. Thus, to assign peptide−drug NOEs we first focused on the isolated NOE peaks that could be assigned unambiguously; an intermediate model was generated once we were able to determine the drug orientation. With aid of the model, we continued to assign additional peptide−drug NOE peaks, even in overlapping areas, based on the network anchoring method.[51−53] Note, however, that ambiguous NOEs have to be supported by other NOEs systematically in this procedure. Models generated using sparse NOEs could be misleading. The $^{1}H-^{1}H$ upper distance constraints between drug and peptide for structure modeling were extracted from the NOESY spectra and listed in Supporting Information Table S3. Models were calculated with those peptide−drug NOEs in addition to distance constraints and backbone dihedral angle constraints from the S31N-WJ332 (**2**) structure.[36] The model structures were computed using XPLOR-NIH.[54]
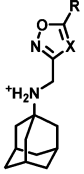
■ RESULTS AND DISCUSSION

Rational Design of Dual Inhibitors Targeting WT and S31N. Previous SAR, structural studies, and MD simulations of drug−M2 interactions revealed a common mechanism of drug action: potent M2 inhibitors, regardless of whether they target WT, S31N, V27A, or L26F, all contain a positively charged ammonium, which presumably serves as a mimic of the conducting hydronium ion that forms water-mediated hydrogen bonds with backbone carbonyls of M2.[36] In addition, channel blockers bind to M2 through hydrophobic interactions and 3-dimensional-shaped (3D-shaped) scaffolds are generally preferred over planar molecules.[55,56,31,57] NMR structural studies of a high-affinity inhibitor of S31N revealed that this inhibitor bound to S31N in a different orientation than previously characterized inhibitors of the WT protein: drugs like amantadine (**1**) and rimantadine bind to WT M2 channel with their positively charged ammonium facing downward toward H37;[47] while M2WJ332 (**2**) bound to the S31N mutant in the opposite orientation with its ammonium facing upward V27.[35,36,58] The orientations of amantadine (**1**) and rimantadine in WT, and M2WJ332 (**2**) in M2-S31N, were modeled by MD simulations, and the orientations were confirmed by solution and solid-state NMR spectroscopies, and further corroborated by SAR studies.[36,47,58] The observed drug-flipping phenomenon provides a rationale for design of dual inhibitors that target both WT and S31N in opposite orientations.

To design such dual inhibitors, we started with our earlier reported inhibitors that had moderate inhibition against both WT and S31N (Table 1).

Table 1. Dual Inhibitors with Moderate Inhibition against Both WT and S31N[a]

Substitution		Compound ID	% WT Inhibition*	% S31N Inhibition*
X = C, R = CH_3,		M2WJ369 (**3**)	55	49
X = N, R = CH_3,		M2WJ405 (**4**)	41	60
X = N, R = H,		M2WJ396 (**5**)	60	52

[a]Asterisk indicates that the values represent the mean of three independent measurements in TEVC assays. We typically see no more than 5% variation in the % inhibition on a given day, or 10% error for measurements made on different days with different batches of oocytes. All compounds were tested at 100 μM.

From the previous SAR studies,[36] we noted that, as the R substitution on the five-membered heterocycles gets bulkier, the WT inhibition of the corresponding compounds decreases drastically. Therefore, to maintain the WT activity, we decided to examine compounds with small R substitutions (e.g., halide, methyl, methoxy). It is also known that a variety of hydrophobic scaffolds are tolerated for WT inhibition,[31,57,59] while adamantane is the preferred moiety for S31N inhibition.[35,36] Thus, we chose adamantane as the hydrophobic scaffold in order to retain S31N activity. With these two criteria in mind, we devised a general structure for the dual inhibitors as shown in Scheme 1. Diversity was introduced at the five-membered heterocycle rings. The linker between adamantane and the heterocycle was kept constant as an ammonium methylene, as it has been shown to be critical for S31N inhibition. On the basis of the binding mode of M2WJ332 (**2**) in S31N mutant as shown in Figure 1, the R group was expected to form hydrophobic interactions with the V27 side chain methyls.

Synthesis and Electrophysiological Testing of Designed Dual Inhibitors. The synthesis of the designed

Scheme 1. Design of Dual Inhibitors Targeting Both WT and S31N

Only small substitution is tolerated for WT inhibition

Designed dual inhibitors

X, Y, Z = C, N, O, S
R = CH₃, F, Cl, Br, I

Critical for S31N inhibition
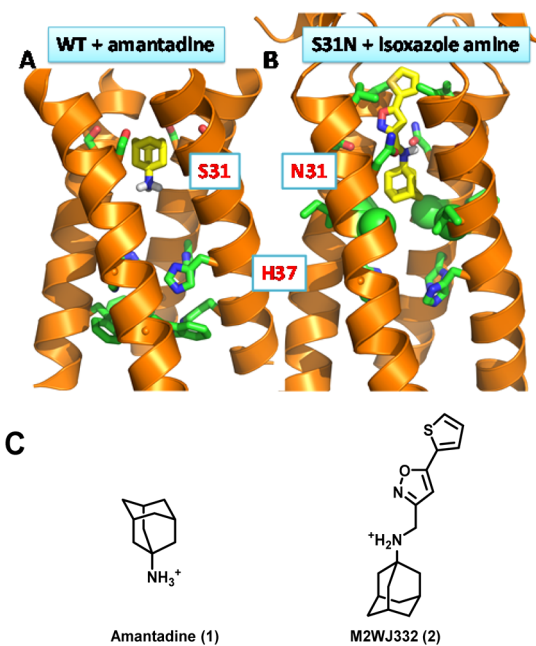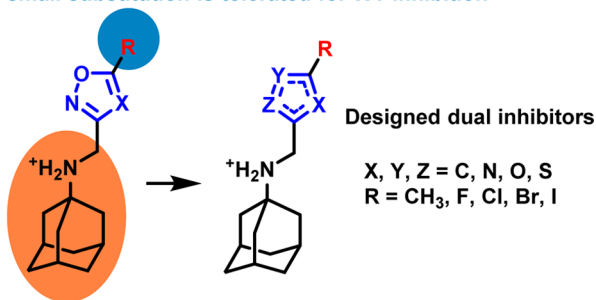
Figure 1. Drug binding orientations in M2-WT and M2-S31N channels. (A) Solid state NMR structure of amantadine-bound WT A/M2 (PDB: 2KQT). Amantadine binds in the channel with its positively charged ammonium facing toward the C-terminal H37. (B) The solution NMR structure of M2WJ332 (**2**)-bound A/M2-S31N (PDB: 2LY0). M2WJ332 (**2**) binds with its positively charged ammonium facing upward the N-terminal V27. (C) Chemical structures of amantadine (**1**) and M2WJ332 (**2**).

Table 2. Initial Screening of Dual Inhibitors Using the TEVC Assays[a]

	R	Compound ID	% S31N inhibition[*]	% WT inhibition[*]
Amantadine		1	36	91
	thiazole-Cl	6	42	56
	1,2,4-thiadiazole-Cl	7	64	54
	thiazole-Br	8	47	28
	thiazole-Br	9	38	36
	isoxazole-Br	10	38	24
	thiophene-Br	11	76	77
	oxazole	12	52	60
	furan	13	6	66
	furan-CH₃	14	37	77
	thiazole-CH₃	15	28	22
	thiazole-NH₂	16	25	38
	thiazole-CH₃	17	36	57
	imidazole-CH₃	18	16	23
	isoxazole-CH₃	19	49	55
	pyrazole-N-CH₃	20	28	13
	1,2,4-isoxazole-CH₃	21	60	41
	1,3,4-oxadiazole-CH₃	22	39	8
	1,3,4-oxadiazole-CF₃	23	33	8
	thiazole-tBu	24	38	5

[a]One asterisk indicates the values that represent the mean of three independent measurements in TEVC assays. We typically see no more than 5% variation in the % inhibition on a given day, or 10% error for measurements made on different days with different batches of oocytes. All compounds were tested at 100 μM.

compounds is shown in the Supporting Information. Compounds were synthesized with highly efficient reductive amination and alkylation as described earlier.[35,36] All compounds were initially tested in two-electrode voltage clamp assays at 100 μM concentration (Table 2). For the potent compounds, IC_{50}'s were subsequently determined. As discussed previously,[32,60] these measurements are made prior to the establishment of equilibrium due to very slow on and off rates for entry of the bulky drugs into the column and the problems of maintaining cells at low pH for extended periods. Hence the IC_{50} values determined by this procedure are significantly higher than the true binding constants. The most potent compound from the five-membered heterocyclic series was *N*-[(5-bromothiophen-2-yl)methyl]adamantan-1-amine (**11**), which showed 76% and 77% inhibition against S31N and WT M2, respectively. In comparison, the bromo-
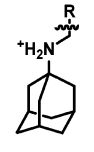
substituted thiazole and isoxazole analogues were less active (**11** versus **8**, **9**, and **10**). Chloro-substituted thiazole (**6**) had moderate activities against both WT and S31N. Interestingly, the chloro-substituted 1,2,4-thiadiazole analogue (**7**) showed improved potency against S31N, and retained its WT inhibition in comparison to **6**. Methyl-substituted compounds were in general less active than their bromo- and chloro-substituted counterparts (**15** versus **6** and **8**). Methyl substitution slightly increased S31N inhibition, but decreased WT inhibition in the case of 1,2,4-isoxazole (**21** versus **12**). Compounds with hydrophilic amine substitution (**16**) and bulky *tert*-butyl substitution (**24**) were inactive against both WT and S31N.

Because the bromo-substituted thiophene **11** had the highest dual inhibition against both WT and S31N, we decided to further explore the SAR. As shown in Table 3, removal of the bromo substitution resulted in drastic decrease of S31N inhibition (**11** versus **25**), presumably due to the lack of favorable hydrophobic interactions with the V27 side chains.

17990

dx.doi.org/10.1021/ja508461m | *J. Am. Chem. Soc.* 2014, 136, 17987−17995

Table 3. Effect of R Substitution on the Potency of Thiophene Inhibitors[a]

R	Compound ID	% S31N inhibition*	% WT(S31) inhibition*	A/WSN/33 (S31N) EC$_{50}$ (μM)	A/Udorn/72 (S31) EC$_{50}$ (μM)	CC$_{50}$** (μM)
Amantadine		36	91	22.5	0.3	>300
H	25	29/N.T.	78/N.T.	N.T.	N.T.	N.T.
Br	11	76/N.T.	77/N.T.	1.8	4.6	123
Cl	26	72/N.T.	91/N.T.	3.5	3.8	133
I	27	85/69	91/72	1.9	4.0	70
CH$_3$	28	73/N.T.	84/N.T.	3.3	9.6	139
OCH$_3$	29	68/N.T.	86/N.T.	3.9	6.8	186
(ethyl)	30	70/N.T.	48/N.T.	N.T.	N.T.	N.T.
(cyclopropyl)	31	77/N.T.	7/N.T.	N.T.	N.T.	N.T.
(4-Br thiophene)	32	45/N.T.	58/N.T.	N.T.	N.T.	N.T.
(3-CH$_3$ thiophene)	33	21/N.T.	71/N.T.	N.T.	N.T.	N.T.
(CH$_3$/Br thiophene)	34	54/N.T.	52/N.T.	N.T.	N.T.	N.T.

[a]One asterisk indicates the values represent the mean of three independent measurements in TEVC assays. We typically see no more than 5% variation in the percent inhibition on a given day, or 10% error for measurements made on different days with different batches of oocytes. All compounds were initially tested at 100 μM. The compounds that showed >80% inhibition at 100 μM were further tested at 30 μM. The data are presented as % inhibition at 100 μM/% inhibition at 30 μM. N.T. = not tested. Two asterisks indicate CC$_{50}$ was measured using confluent monolayer Madin−Darby canine kidney (MDCK) epithelial cells. Cell viability was quantified after 72 h by MTT.[61]

However, removal of the bromo substitution had no effect on the WT inhibition (**11** versus **25**). Other halides such as chloro and iodo were similarly tolerated in the same position, and the resulting compounds retained potent inhibition against both WT and S31N (**11** versus **26** and **27**). All potent compounds were also tested in plaque reduction assays. The EC$_{50}$s of 5-halide-substituted adamantyl thiophene amines (**11**, **26**, and **27**) all fell in the single digit low micromolar range. Methyl-substituted thiophene (**28**) was 2-fold less active than its bromo analogue (**11**) in inhibiting both WT and S31N. Methoxy substitution at the same position also resulted in a less active compound (**29**). Compounds with ethyl (**30**) and cyclopropyl (**31**) substitutions showed drastic decrease in WT inhibition, while having little or no effect on their S31N inhibition. Collectively, the SAR correlates with the design rationale in which a bulky R group is not tolerated in WT inhibition. Moving the substitutions from the 5-position of the thiophene to the 4-position (**32**) or the 3-position (**33**) led to the loss of activity against both WT and S31N, suggesting the binding geometry of the drug is important. Introducing an extra methyl at the 4-position also decreased the activity (**11** versus **34**). Cellular cytotoxicity of the active dual inhibitors, **11**, **26**, **27**, **28**, and **29**, were profiled using the 3-(4, 5-dimethylthiazolyl-2)-2,5-diphenyltetrazolium bromide (MTT) assay.[61] The CC$_{50}$ values were in the range 145−196 μM. The selectivity index for the most potent dual inhibitors, **11** and **27**, were >37, rendering them as promising candidates to be further pursued in the following *in vivo* mouse studies.

NMR Studies of the Dual Inhibitor 11 Binding to WT and S31N M2. Our design was based on the idea that dual inhibitors bind to WT and S31N in opposite orientations. To experimentally validate this hypothesis of flip-flop drug binding, we recorded solution NMR NOESY spectra to determine drug-M2-TM interactions. Synthetic peptides with ^{15}N−^{13}C−labeled amino acids at selected positions were used for this study in order to simplify the spectrum and obtain unambiguous drug-M2-TM NOEs. The channel-forming transmembrane peptide corresponding to the pore of WT M2 is denoted WT (19−49) VASIGH, meaning residues at V27, A30, S31, I33, G34, and H37 are uniformly ^{15}N−^{13}C−labeled. For the S31N (19−49) VANIG peptide, residues at V27, A30, N31, I33, and G34 are uniformly ^{15}N−^{13}C−labeled. The chemical shifts for the complexes of WT VASIGH and S31N VANIG in the presence of **11** were very similar to those observed for the amantadine-bound WT M2 TM[47] and the M2WJ332 (**2**)-bound S31N,[36] respectively. Assignments were obtained by direct comparison and confirmed by 2D C(C)H-TOCSY, and assignments of I33 and V27 are labeled in Supporting Information Figure S3. Two-dimensional ^{13}C-edited NOESY experiments with 150 ms mixing time were used to identify peptide−drug NOEs for S31N (19−49) VANIG peptide (Figure 2A) and the WT (19−49) VASIGH peptide (Figure 2B).

The assignment of the complex of S31N (19−49) VANIG in complex with **11** (Figure 2A) is similar to that used previously to solve the corresponding complex with M2WJ332 (**2**).[36] NOE peaks between G34 Cα and the drug protons H7 and H8

A S31N (19-49) VANIG
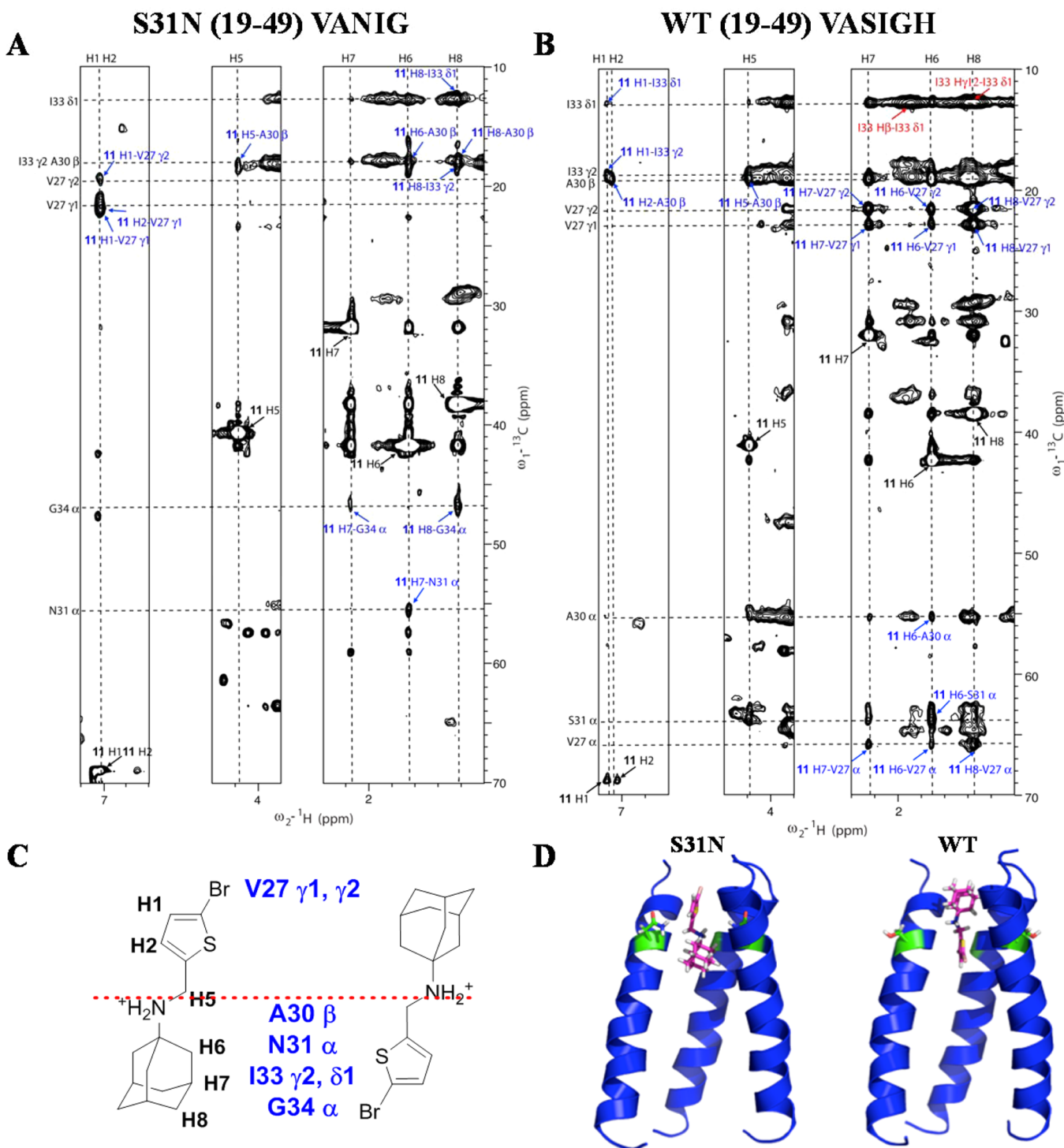
B WT (19-49) VASIGH

Figure 2. Flip-flop orientation of **11** in M2. (A) 2D ^{13}C−^{1}H NOESY (150 ms) experiment for S31N (19−49) VANIG sample in the presence of **11**. (B) 2D ^{13}C−^{1}H NOESY (150 ms) experiment for WT (19−49) VASIGH sample in the presence of **11**. Assignments for drug−peptide cross peaks are labeled in blue and listed in Supporting Information Table S3. Assignments for peptide−peptide cross peaks are labeled in red. The diagonal peaks from the drug are labeled in black. (C) Illustration of relative position of **11** in S31N and WT, based on intermolecular peptide−drug NOEs. (D) Models calculated with the same peptide−drug NOEs in addition to distance constraints for the peptide obtained for S31N-WJ332 structure. Left is for S31N, and right is for WT in both parts C and D. Positions of the dual inhibitor **11** in S31N and WT are flipped and mirrored along residue 31, providing a direction to design an inhibitor for all M2 mutants. Models generated using the drug-M2 NOEs were deposited in PDB with codes of 2MUW and 2MUV for drug-bound WT-M2 and the S31N mutant, respectively.

were assigned straightforwardly because the Cα chemical shift of Gly is very unique and easily identified. Chemical shifts of drug protons H1 and H2 are overlapped, but the two protons have strong NOEs to the V27 methyl groups that do not

overlap with any other peaks, clearly showing that the Val27 methyl groups and the thiophene ring of **11** are very close in space. These NOEs unambiguously demonstrate the drug is up in the S31N channel. Next, the isolated peak of N31 Cα and

the drug H6 was assigned. Furthermore, additional NOE assignments for peaks that were overlapped with another were assigned on the basis of the network anchoring approach[51−53] with aid of the intermediate models.

Similarly, for the WT (19−49) VASIGH sample, we began with the NOE peaks that could be assigned unambiguously (Figure 2B). A cross-peak between I33 methyl groups and the thiophene ring (**11** H1 to I33 γ2 and δ1), together with the *lack* of NOEs to Val27 methyl groups (as were the case for S31N), place the aromatic group pointing down into the channel. Additionally, NOEs between V27 methyl groups and the adamantane protons H6, H7, and H8 indicate that the adamantane is located near the N-terminus. At this stage, we generated an intermediate model, which aided the assignment of additional peptide−drug NOEs. From the adamantane protons (H6, H7, and H8), we assigned NOEs to the Cα atoms of V27, A30, and S31. NOEs were also assigned between the thiophene proton H2 and the methylene protons H5 from the drug **11** and the methyl group of Ala30, respectively.

For the WT (19−49) VASIGH sample, we also observed a series of NOEs from the I33 δ1 methyl and a number of aliphatic protons, near the chemical shifts of adamantane protons (upper right of Figure 2B). We were unable to assign this region of the spectrum, because it is heavily congested with intraresidue NOEs from I33 as well as NOEs to other regions of the protein (the NOEs seen in a ^{13}C-filtered experiment do not differentiate signals from drug versus other protons in the protein). Given the heavy congestion of the spectrum in this region, we could not rule out the possibility of NOEs from drug **11** to I33, which would have been consistent with the drug binding with thiophene in the up orientation. However, the lack of *systematic* NOEs between the thiophene protons (H1 and H2) and V27 as were seen in the complex with S31N (19−49) VANIG (Figure 2A) together with the presence of NOEs locating the thiophene ring in the channel near Ala30 indicate that **11** is primarily bound with the heteroaryl group pointing down. Thus, while we are unable to rule out the possibility of other minor conformers, these data clearly confirm that the predominant orientation for WT is with the adamantane up near Val27 and the thiophene directed downward.

These peptide−drug NOEs, along with the distance constraints and backbone dihedral angle constraints for defining the peptide's tetrameric structure obtained for the S31N-M2WJ332 (**2**) structure,[36] were used to build the models using XPLOR-NIH[54] as shown in Figure 2D. There were no distance violations (>0.5 Å) for the assigned NOEs.

MD Simulations of the Dual Inhibitor 11 Binding to WT and S31N. We used MD simulations of M2-TM in a phospholipid bilayer to investigate the dual inhibitory behavior adopted by compound **11** against the M2 proton channels (both WT and S31N mutant) (Figure 3). Given the very slow on and off rates of amantadine derivatives (typically on the hour time scale[32,60]), the extended structure of the inhibitor, and the restricted geometry of the pore, it was necessary to initiate the simulations with the molecule already inserted in the pore in the predominant orientation inferred from solution NMR. In both simulations, the ammonium gradually converges to stable positions along the pore. In the WT M2-TM, we initialized compound **11** to minimize steric clashes: during the first tens of nanoseconds, the ammonium's position shifts by about 1 Å toward V27 and aligns itself with the backbone carbonyl of G34, which is the native binding mode for amantadine.[33,40] The movement of **11** toward its final pose is
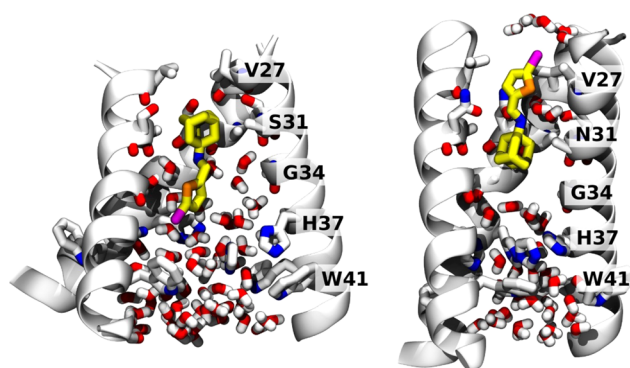
Figure 3. Final MD snapshots of compound **11** bound to the transmembrane segment of WT and S31N M2 in a lipid bilayer. Left: **11** bound within WT M2 after 200 ns. Right: **11** bound within S31N M2 after 100 ns. The protein backbone is shown as ribbons; pore-lining side chains and backbone carbonyls, ligand, and water molecules within the pore are shown as sticks. Water molecules solvating the bromine atom in the outward-facing pose (right) are also shown.

accompanied by a conformational change of the M2-TM backbone, in the direction toward the low pH structure.[62] After 200 ns, the root-mean-square deviation (RMSD) of the backbone atoms from the starting structure[42] is 4 Å, whereas the RMSD from the low pH structure[62] is 2.5 Å. For comparison, MD simulations of the stable drug-free or inhibitor-bound conformation yield RMSDs of approximately 1 Å, attributable to thermal fluctuations:[33,42] therefore, the final structure is similar to, but distinct from, the low pH structure.[62] A similar conformational change was also observed in phospholipid bilayers as an effect of mutations of D44.[63] Close interactions are formed between the phosphate groups of the lipids with R45, and water molecules between V27 side chains disappear altogether. Within the pore, the bromine atom of **11** forms transient, nonspecific interactions with water molecules, the backbone carbonyl of G34, and the imidazole of H37: this is in agreement with the ranking of the binding energies with these three moieties in quantum mechanical calculations (see Supporting Information).

In the S31N mutant, we initialized **11** with the bromo-thiophene moiety facing toward V27, and the ammonium aligned with the side chain of N31, as in the S31N-M2WJ332 (**2**) structure (PDB: 2LY0).[36] This position is maintained throughout the simulation. The V27 side chains are packed tightly around the thiophene group in the starting structure: the C_γ atoms from opposite monomers are separated by 7.8 Å. During the first 100 ns, the N-terminal residues slightly expand to accommodate the thermal fluctuations of **11** (the separation between opposing C_γs increases to 9.2 Å). Water molecules that are initially positioned around **11** leave the region between V27 and G34, with the exception of two water molecules coordinating the ammonium group, also seen in the previous S31N-M2WJ332 (**2**) simulations.[36] In this binding mode, the bromine atom is surrounded by the V27 side chains, and only partially exposed to the outer solvent: the pair correlation function with water oxygens (see Supporting Information) shows 4 or 5 water molecules weakly interacting with the bromine. The first hydration shell is centered at 3.5 Å of distance from the bromine, while the second appears as an even broader peak centered at 6 Å (integrals at 5 and 8 Å, respectively): both features resemble very closely those of a methyl group at an oil−water interface.[64] This mode of

interaction is in agreement with the SAR of molecules with bromine substituted by other halogens, as well as a methyl (Table 3).

In summary, the drug binding orientation of dual inhibitor **11** as inferred from solution NOEs are supported by MD simulations, showing the relative orientations were indeed stable within the simulation time.

CONCLUSIONS

The heterogeneity of influenza viruses poses a great challenge in the development of anti-influenza drugs. For effective neutralization of influenza viruses, influenza vaccines normally contain two strains of influenza A viruses, A/California/7/2009 (H1N1)-like virus and A/Texas/50/2012 (H3N2) virus, plus at least one strain of influenza B virus, typically B/Massachusetts/2/2012.[65] Although influenza vaccines remain the cornerstone in prophylaxis of influenza infection, they are much less active than small molecule antivirals in treating influenza-infected patients.[66] Moreover, due to antigenic shift and antigenic drift of influenza viruses, influenza vaccines have to be reformulated each year; plus, there is generally a six-month delay in vaccine production. The limitations of influenza vaccines together with the heterogeneous makeup of influenza viruses call for broad-spectrum small molecule antivirals. We designed a class of such broad-spectrum dual inhibitors with EC_{50} values against WT and M2 S31N influenza viruses, which is comparable with that of amantadine (**1**) in inhibiting WT influenza virus. Our design was based on the hypothesis that dual inhibitors bind to WT and M2-S31N channels with opposite orientations: the aromatic headgroup faces down toward the C-termini and toward N-terminus in WT and S31N channel, respectively. Starting with our previously discovered lead compounds showing moderate dual inhibition, we identified halide-substituted thiophene compounds having the highest potencies. The antiviral activity of the most potent inhibitor, **11**, in inhibiting WT and the S31N mutant is on par with that of amantadine (**1**) in inhibiting WT virus. NMR investigations were also consistent with the guiding rationale for inhibitor design. All unambiguous NOEs indicated that the inhibitors bind to the WT and S31N channels in opposite orientations, although we cannot rule out the possibility of other minor conformational states of the drug in the WT protein due to spectral overlap. The dual inhibitors reported herein provide promising lead compounds for further medicinal chemistry optimization with the ultimate goal of developing broad-spectrum anti-influenza drugs.

ASSOCIATED CONTENT

Ⓢ Supporting Information

Synthesis procedures, compound characterizations, quantum chemical calculations, and molecular dynamics simulation details. This material is available free of charge via the Internet at http://pubs.acs.org.

AUTHOR INFORMATION

Corresponding Authors

junwang@pharmacy.arizona.edu
giacomo.fiorin@temple.edu
william.degrado@ucsf.edu

Author Contributions

○Y.W., B.C., and H.J. contributed equally.

Notes

ACKNOWLEDGMENTS

REFERENCES

(1) Cox, N.; Subbarao, K. *Annu. Rev. Med.* **2000**, *51*, 407.
(2) Thompson, W.; Shay, D.; Weintraub, E.; Brammer, L.; Cox, N.; Anderson, L.; Fukuda, K. *JAMA, J. Am. Med. Assoc.* **2003**, *289*, 179.
(3) Thompson, W.; Shay, D.; Weintraub, E.; Brammer, I.; Bridges, C.; Cox, N.; Fukuda, K. *JAMA, J. Am. Med. Assoc.* **2004**, *292*, 1333.
(4) Abdel-Ghafar, A.; Chotpitayasunondh, T.; Gao, Z.; Hayden, F.; Hien, N.; de Jong, M.; Naghdaliyev, A.; Peiris, J.; Shindo, N.; Soeroso, S.; Uyeki, T.; Consultation, n. W. H. O.; Consultation, n. W. H. O. *N. Engl. J. Med.* **2008**, *358*, 261.
(5) Yu, H.; Cowling, B. J.; Feng, L.; Lau, E. H.; Liao, Q.; Tsang, T. K.; Peng, Z.; Wu, P.; Liu, F.; Fang, V. J.; Zhang, H.; Li, M.; Zeng, L.; Xu, Z.; Li, Z.; Luo, H.; Li, Q.; Feng, Z.; Cao, B.; Yang, W.; Wu, J. T.; Wang, Y.; Leung, G. M. *Lancet* **2013**, *382*, 138.
(6) Xu, R.; McBride, R.; Nycholat, C.; Paulson, J.; Wilson, I. *J. Virol.* **2012**, *86*, 982.
(7) Das, K. *J. Med. Chem.* **2012**, *55*, 6263.
(8) Samson, M.; Pizzorno, A.; Abed, Y.; Boivin, G. *Antiviral Res.* **2013**, *98*, 174.
(9) Cheng, P.; Leung, T.; Ho, E.; Leung, P.; Ng, A.; Lai, M.; Lim, W. *Emerg. Infect. Dis.* **2009**, *15*, 966.
(10) Moscona, A. *N. Engl. J. Med.* **2005**, *353*, 1363.
(11) Boltz, D.; Aldridge, J.; Webster, R.; Govorkova, E. *Drugs* **2010**, *70*, 1349.
(12) *WHO Guidelines for Pharmacological Management of Pandemic Influenza A(H1N1) 2009 and Other Influenza Viruses*; World Health Organization: Geneva, Feb 2010. Available from http://www.ncbi.nlm.nih.gov/books/NBK138515/.
(13) Ison, M. *Curr. Opin. Virol.* **2011**, *1*, 563.
(14) Tsiodras, S.; Mooney, J.; Hatzakilis, A. *BMJ [Br. Med. J.]* **2007**, *334*, 293.
(15) Webster, R. G.; Govorkova, E. A. *Ann. N.Y. Acad. Sci.* **2014**, *1323*, 115.
(16) Cheung, C.; Rayner, J.; Smith, G.; Wang, P.; Naipospos, T.; Zhang, J.; Yuen, K.; Webster, R.; Peiris, J.; Guan, Y.; Chen, H. *J. Infect. Dis.* **2006**, *193*, 1626.
(17) Hayden, F. *Influenza Other Respir. Viruses* **2013**, *7*, 63.
(18) Pinto, L.; Lamb, R. *J. Biol. Chem.* **2006**, *281*, 8997.
(19) Wang, J.; Qiu, J. X.; Soto, C.; DeGrado, W. F. *Curr. Opin. Struct. Biol.* **2011**, *21*, 68.
(20) Hay, A.; Wolstenholme, A.; Skehel, J.; Smith, M. *EMBO J.* **1985**, *4*, 3021.
(21) Brown, A. N.; McSharry, J. J.; Weng, Q.; Driebe, E. M.; Engelthaler, D. M.; Sheff, K.; Keim, P. S.; Nguyen, J.; Drusano, G. L. *Antimicrob. Agents Chemother.* **2010**, *54*, 3442.
(22) Grambas, S.; Hay, A. J. *Virology* **1992**, *190*, 11.
(23) Shiraishi, K.; Mitamura, K.; Sakai-Tagawa, Y.; Goto, H.; Sugaya, N.; Kawaoka, Y. *J. Infect. Dis.* **2003**, *188*, 57.
(24) Abed, Y.; Goyette, N.; Boivin, G. *Antimicrob. Agents Chemother.* **2005**, *49*, 556.
(25) Balannik, V.; Carnevale, V.; Fiorin, G.; Levine, B.; Lamb, R.; Klein, M.; DeGrado, W.; Pinto, L. *Biochemistry* **2010**, *49*, 696.
(26) Stouffer, A. L.; Ma, C.; Cristian, L.; Ohigashi, Y.; Lamb, R. A.; Lear, J. D.; Pinto, L. H.; DeGrado, W. F. *Structure* **2008**, *16*, 1067.
(27) Suzuki, H.; Saito, R.; Masuda, H.; Oshitani, H.; Sato, M.; Sato, I. *J. Infect. Chemother.* **2003**, *9*, 195.

(28) Furuse, Y.; Suzuki, A.; Kamigaki, T.; Oshitani, H. *Virol. J.* **2009**, *6*, 67.

(29) Furuse, Y.; Suzuki, A.; Oshitani, H. *Antimicrob. Agents Chemother.* **2009**, *53*, 4457.

(30) Das, K.; Aramini, J.; Ma, L.; Krug, R.; Arnold, E. *Nat. Struct. Mol. Biol.* **2010**, *17*, 530.

(31) Rey-Carrizo, M.; Torres, E.; Ma, C.; Barniol-Xicota, M.; Wang, J.; Wu, Y.; Naesens, L.; DeGrado, W. F.; Lamb, R. A.; Pinto, L. H.; Vazquez, S. *J. Med. Chem.* **2013**, *56*, 9265.

(32) Balannik, V.; Wang, J.; Ohigashi, Y.; Jing, X.; Magavern, E.; Lamb, R. A.; DeGrado, W. F.; Pinto, L. H. *Biochemistry* **2009**, *48*, 11872.

(33) Wang, J.; Ma, C.; Fiorin, G.; Carnevale, V.; Wang, T.; Hu, F.; Lamb, R. A.; Pinto, L. H.; Hong, M.; Kein, M. L.; DeGrado, W. F. *J. Am. Chem. Soc.* **2011**, *133*, 12834.

(34) Wang, J.; Ma, C.; Wu, Y.; Lamb, R. A.; Pinto, L. H.; DeGrado, W. F. *J. Am. Chem. Soc.* **2011**, *133*, 13844.

(35) Wang, J.; Ma, C.; Wang, J.; Jo, H.; Canturk, B.; Fiorin, G.; Pinto, L. H.; Lamb, R. A.; Klein, M. L.; DeGrado, W. F. *J. Med. Chem.* **2013**, *56*, 2804.

(36) Wang, J.; Wu, Y.; Ma, C.; Fiorin, G.; Wang, J.; Pinto, L. H.; Lamb, R. A.; Klein, M. L.; DeGrado, W. F. *Proc. Natl. Acad. Sci. U.S.A.* **2013**, *110*, 1315.

(37) Sharma, M.; Yi, M.; Dong, H.; Qin, H.; Peterson, E.; Busath, D. D.; Zhou, H.-X.; Cross, T. A. *Science* **2010**, *330*, 509.

(38) Miao, Y.; Qin, H.; Fu, R.; Sharma, M.; Can, T. V.; Hung, I.; Luca, S.; Gor'kov, P. L.; Brey, W. W.; Cross, T. A. *Angew. Chem., Int. Ed.* **2012**, *51*, 8383.

(39) Andreas, L. B.; Eddy, M. T.; Chou, J. J.; Griffin, R. G. *J. Am. Chem. Soc.* **2012**, *134*, 7215.

(40) Cady, S. D.; Schmidt-Rohr, K.; Wang, J.; Soto, C. S.; DeGrado, W. F.; Hong, M. *Nature* **2010**, *463*, 689.

(41) De Clercq, E. *Nat. Rev. Drug Discovery* **2007**, *6*, 1001.

(42) Acharya, R.; Carnevale, V.; Fiorin, G.; Levine, B. G.; Polishchuk, A. L.; Balannik, V.; Samish, I.; Lamb, R. A.; Pinto, L. H.; DeGrado, W. F.; Klein, M. L. *Proc. Natl. Acad. Sci. U.S.A.* **2010**, *107*, 15075.

(43) Klauda, J. B.; Venable, R. M.; Freites, J. A.; O'Connor, J. W.; Tobias, D. J.; Mondragon-Ramirez, C.; Vorobyov, I.; MacKerell, A. D.; Pastor, R. W. *J. Phys. Chem. B* **2010**, *114* (23), 7830−7843.

(44) MacKerell, A. D.; Brooks, B.; Brooks, C. L.; Nilsson, L.; Roux, B.; Won, Y.; Karplus, M. CHARMM: The Energy Function and Its Parameterization. In *Encyclopedia of Computational Chemistry*; John Wiley & Sons: New York, 2002.

(45) Vanommeslaeghe, K.; Hatcher, E.; Acharya, C.; Kundu, S.; Zhong, S.; Shim, J.; Darian, E.; Guvench, O.; Lopes, P.; Vorobyov, I.; MacKerell, A. D. *J. Comput. Chem.* **2010**, *31*, 671.

(46) Jorgensen, W. L.; Chandrasekhar, J.; Madura, J. D.; Impey, R. W.; Klein, M. L. *J. Chem. Phys.* **1983**, *79*, 926.

(47) Cady, S. D.; Wang, J.; Wu, Y.; DeGrado, W. F.; Hong, M. *J. Am. Chem. Soc.* **2011**, *133*, 4274.

(48) Sattler, M.; Schleucher, J.; Griesinger, C.; Smith, M. E.; Eck, E. R. H. v. *Heteronuclear Multidimensional NMR Experiments for the Structure Determination of Proteins in Solution Employing Pulsed Field Gradients*; Elsevier: Amsterdam, 1999.

(49) Cavanagh, J.; Fairbrother, W. J.; Palmer, A. G., III; Rance, M.; Skelton, N. J. *Protein NMR Spectroscopy: Principles and Practice*; Academic Press: Amsterdam; Boston, 2007.

(50) Delaglio, F.; Grzesiek, S.; Vuister, G. W.; Zhu, G.; Pfeifer, J.; Bax, A. *J. Biomol. NMR* **1995**, *6*, 277.

(51) Nilges, M.; Macias, M. J.; O'Donoghue, S. I.; Oschkinat, H. *J. Mol. Biol.* **1997**, *269*, 408.

(52) Huang, Y. J.; Tejero, R.; Powers, R.; Montelione, G. T. *Proteins.* **2006**, *62*, 587.

(53) Herrmann, T.; Güntert, P.; Wüthrich, K. *J. Mol. Biol.* **2002**, *319*, 209.

(54) Schwieters, C. D.; Kuszewski, J. J.; Tjandra, N.; Marius Clore, G. *J. Magn. Reson.* **2003**, *160*, 65.

(55) Lagoja, I. M.; De Clercq, E. *Med. Res. Rev.* **2008**, *28*, 1.

(56) Wanka, L.; Iqbal, K.; Schreiner, P. *Chem. Rev.* **2013**, *113*, 3516.

(57) Duque, M. D.; Ma, C.; Torres, E.; Wang, J.; Naesens, L.; Juarez-Jimenez, J.; Camps, P.; Javier Luque, F.; DeGrado, W. F.; Lamb, R. A.; Pinto, L. H.; Vazquez, S. *J. Med. Chem.* **2011**, *54*, 2646.

(58) Williams, J. K.; Tietze, D.; Wang, J.; Wu, Y.; DeGrado, W. F.; Hong, M. *J. Am. Chem. Soc.* **2013**, *135*, 9885.

(59) Wang, J.; Ma, C.; Balannik, V.; Pinto, L. H.; Lamb, R. A.; DeGrado, W. F. *ACS Med. Chem. Lett.* **2011**, *2*, 307.

(60) Wang, C.; Takeuchi, K.; Pinto, L. H.; Lamb, R. A. *J. Virol.* **1993**, *67*, 5585.

(61) Torres, E.; Duque, M. D.; Vanderlinden, E.; Ma, C.; Pinto, L. H.; Camps, P.; Froeyen, M.; Vázquez, S.; Naesens, L. *Antiviral Res.* **2013**, *99*, 281.

(62) Stouffer, A. L.; Acharya, R.; Salom, D.; Levine, A. S.; Di Costanzo, L.; Soto, C. S.; Tereshko, V.; Nanda, V.; Stayrook, S.; DeGrado, W. F. *Nature* **2008**, *451*, 596.

(63) Ma, C.; Fiorin, G.; Carnevale, V.; Wang, J.; Lamb, R. A.; Klein, M. L.; Wu, Y.; Pinto, L. H.; DeGrado, W. F. *Structure* **2013**, *21*, 2033.

(64) Ashbaugh, H. S.; Paulaitis, M. E. *J. Am. Chem. Soc.* **2001**, *123*, 10721.

(65) Grohskopf, L.; Shay, D.; Shimabukuro, T.; Sokolow, L.; Keitel, W.; Bresee, J.; Cox, N. *MMWR Recomm. Rep.* **2013**, *62*, 1.

(66) Jin, H.; Chen, Z. *Curr. Opin. Virol.* **2014**, *6*, 34.